Engineering hierarchical nanochannels in graphene oxide membranes by etching and polydopamine intercalation for highly efficient dye recovery

Xiaoyi Chen[a,†], Erda Deng[a,†], Xiaoci Lin[a], Ameya Manoj Tandel[a], Darius Rub[a], Lingxiang Zhu[b,c], Liang Huang[a], and Haiqing Lin[a]*

[a]Department of Chemical and Biological Engineering, University at Buffalo, The State University of New York, Buffalo, NY 14260, United States

[b]Department of Energy, National Energy Technology Laboratory, 626 Cochrans Mill Road, P.O. Box 10940, Pittsburgh, PA 15236, United States

[c]NETL Support Contractor, 626 Cochrans Mill Road, P.O. Box 10940, Pittsburgh, PA 15236, United States

[†] X.C. and E.D. contributed equally to this work.

* Corresponding author. Tel: +1-716-645-1856, Email: haiqingl@buffalo.edu (H. Lin)

ABSTRACT

Graphene oxide (GO) membranes have been extensively investigated for dye removal from wastewater, and they are often reduced or cross-linked to improve their stability, which, however, decreases water permeance. This study demonstrates an effective approach to enhance both durability and water permeance and retain dye rejection by synergistically integrating chemical etching using H_2O_2 and intercalation with polydopamine (PDA) to create hierarchical nanochannels. The nanopores on the holey GO (HGO) shorten the diffusion path, while the PDA intercalation increases the channel sizes and stabilizes the GO nanosheets. Optimized membranes exhibit water permeance of 70 - 120 LMH/bar (much higher than state-of-the-art commercial polyamide membranes) and a Congo Red rejection of 98.5%, better than GO membranes reported in the literature. Moreover, a membrane with water permeance of 70 LMH/bar exhibits stable performance in a 3-day continuous crossflow filtration test. The versatile approach reported here may be applied to other two-dimensional materials to create hierarchical nanochannels for desired separations.

KEYWORDS*:* Membranes; Dye removal; Holey graphene oxide; Polydopamine intercalation; Chemical etching

1. Introduction

The steady increase of the demand for textiles and apparel has significantly increased the use of dyes, and their release in wastewater has caused serious water pollution. Dye recovery from wastewater is an effective way to mitigate pollution and reuse valuable dyes [1-5]. Membrane technology has attracted significant interest for dye recovery from wastewater due to its inherently high energy efficiency, low cost, small footprint, and absence of chemical wastes [6, 7]. For example, state-of-the-art commercial nanofiltration (NF) membranes based on polyamides exhibit high rejection to dyes because their pore sizes are usually smaller than dyes and water permeance of ~ 10 L m^{-2} h^{-1} bar^{-1} (LMH/bar) [1, 8, 9]. However, as textile wastewater often contains salts (such as Na_2SO_4), which are used to improve the dye uptake by textiles, conventional NF membranes can exhibit high salt rejection, increasing the osmotic pressure and thus operating pressure required for water permeation. Tight ultrafiltration (UF) membranes with high salt and water permeance have also been considered, but the dye rejection is often not sufficiently high [10]. There is an imperative need to develop new membranes with high water permeance, high dye rejection, low salt rejection, and good long-term stability.

Two-dimensional (2D) graphene oxide (GO) has emerged as an exciting platform to construct membranes with tunable channel sizes with a sharp molecular-sieving ability [11-16]. The nanosheets of 1 μm or larger can form a laminar structure with sub-nanometer interlayer spacing, achieving high dye/salt separation properties [2, 3]. However, GO membranes face two significant challenges for industrial implementation. First, the nanosheets have aspect ratios as high as ~2000, leading to an extremely high tortuosity for the transport of small molecules [17]. The membranes can be fabricated as thin as nanometers to improve water permeance or processed by solvation to manipulate nanochannels [2, 3, 18], but the ability to produce defect-free membranes at a large scale is yet to be demonstrated. On the other hand, creating nanopores on the nanosheets by etching to obtain holey GO (HGO) has been demonstrated to be an effective and facile way to decrease the tortuosity [15, 19, 20]. For example, etching of the GO sheets using H_2O_2 increased water permeance from 0.4 to 6.6 LMH/bar by 16 times (consistent with the theoretical modeling), though the etching had a minimal effect on the interlayer spacings [15].

The second challenge arises from the hydrophilicity of the GO, leading to their good dispersibility in water and thus instability for long-term underwater operation [12, 21]. The oxygen-containing groups of the GO can be removed to increase hydrophobicity (i.e., reduction) and thus stability in the water using chemicals, such as N_2H_4 [3, 22], HI [15], and polydopamine (PDA) [23, 24]. However, the reduction decreases interlay spacing and thus water permeance [25]. Another way to impart stability is cross-linking GOs using diamines [21] or cations [26]. Particularly, PDA, a bio-adhesive material that can be deposited on a variety of surfaces [27, 28], can stabilize the GO layers onto the porous support [29] or serve as a protective layer on top of the GO layer to improve the GO stability [30-33]. More importantly, PDA can cross-link adjacent nanosheets [21, 34-36], in addition to the reduction [23, 24], though the bridging and reduction decreased the channel size and water permeance. However, the cross-linking reaction requires 24 h at ≈65 °C [24, 37], which is time-consuming and may form PDA nanoparticles of 100 nm or larger [28], disrupting the stacking of the nanosheets and making the membrane unstable.

This study represents the first effort in integrating chemical etching and PDA-intercalation of the GO nanosheets to improve water permeance, dye recovery efficiency, and underwater stability, as shown in Figure 1. The etching decreases the tortuosity of the GO layer, and the PDA intercalation stabilizes the GO layer and increases the nanochannel size and thus water and salt permeance while retaining the dye rejection. Specifically, GO nanosheets were etched using H_2O_2 to form HGO, which was then mixed with dopamine before being deposited onto a porous support. The membranes were thoroughly characterized for chemical and structural properties, including morphology, elemental information, thickness, and molecular weight cutoff (MWCO). The PDA/HGO membranes exhibit water permeance one order magnitude higher than state-of-the-art NF membranes, higher salt permeance, and comparable dye retention. The membranes with the most promising separation properties were challenged with a 3-day continuous crossflow filtration test. The stable dye retention indicates the integrity of the membranes and their potential for practical applications.

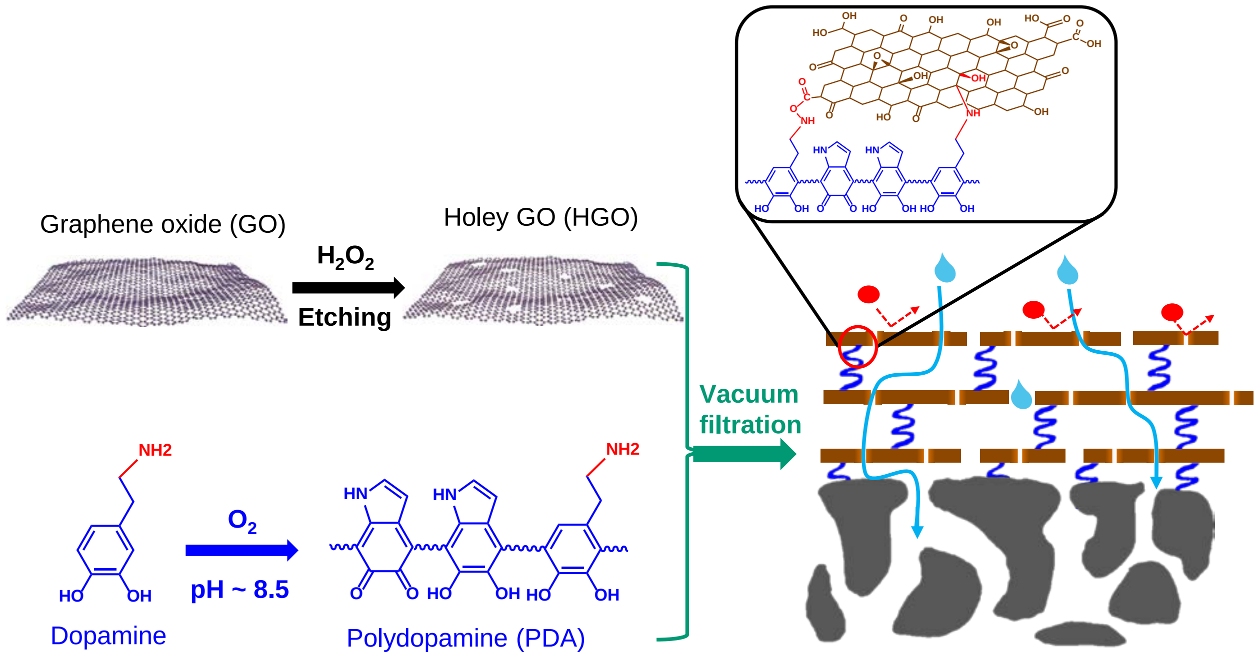

Fig. 1. Schematic of the synthesis of PDA/HGO membranes, including chemical etching of GO with H_2O_2 and the use of PDA to stabilize the nanosheets and adhere them to the porous support. The blue drop represents salty water, and the red circle indicates dye molecules.

2. Experimental

2.1. Materials

Natural graphite powder (325 mesh) was obtained from Qingdao Huatai Graphite Co. (Qingdao, China). H_2O_2 (30 wt.% in H_2O), H_2SO_4 (99%), $KMnO_4$ (≥99.0%), dopamine hydrochloride, Trizma base (≥99.9 %), Congo red (CR, 697 Da), Direct red 80 (DR 80, 1373 Da), poly(ethylene glycol) (PEG), and Na_2SO_4 (≥99.0 %) were purchased from Sigma-Aldrich Corporation (St. Louis, MO). HCl (2.0 M) and dimethylformamide (DMF, ≥99.8 %) were obtained from VWR International (Radnor, PA). Polyethersulfone (PES) microfiltration (MF) membrane with a pore size of 50 nm (MP005) was supplied by Sterlitech (Kent, WA). Methyl blue (MB, 800

Da) and isopropanol (IPA, 99.6%) were acquired from Fisher Scientific International (Pittsburgh, PA).

2.2. Preparation of PDA/GO and PDA/HGO membranes

GO was prepared from graphite using the modified Hummers' method [3, 15]. HGO was prepared by adding H_2O_2 (10 mL) to 2 g/L GO solution (100 mL), followed by continuous agitation at 100 °C for 2 or 4 h. The oxidation generates nanopores on the HGO nanosheets and reduces nanosheet sizes [15, 20, 38]. The product was denoted as HGO2h and HGO4h based on the etching time. Finally, the HGO solution was purified by dialysis to remove the residual H_2O_2. To study the effect of the HGO nanosheet size on the membrane performance, a portion of the HGO solution was further centrifuged, and the supernatant containing small HGO debris was discarded. The large HGO nanosheets are denoted as HGO2hC or HGO4hC.

The PDA/GO and PDA/HGO membranes were prepared by vacuum filtration [3, 20]. First, dopamine was added to the GO aqueous solution, followed by sonication in an ice bath for 1 h. The weight ratio between dopamine and GO was 2:1, while the amount of GO in the solution was monitored to prepare the membranes with various thicknesses. The PES support membrane was pretreated using IPA for 10 min and then immersed in DI water before use. The PDA/GO solution was then vacuum filtrated onto the PES support to form the membrane. To stabilize the membrane, filtration was continued with water for another hour, and the obtained membrane was kept in DI water. The PDA/HGO membranes were prepared using the same approach except that HGO was used instead of GO. The membranes were denoted as PDA/*x*-*y*, where *x* can be GO, HGO2h, or HGO4h used, and *y* is the determined thickness (nm) of the selective layer.

2.3. Characterization of GO and membranes

The morphology of GO, HGO, and membranes was characterized using a focused ion beam scanning electron microscope (FIB-SEM, Carl Zeiss Auriga CrossBeam, Carl Zeiss, Germany). The hydrophilicity of the membrane surface was characterized using a Ramé Hart contact angle goniometer (Model 190, Succasunna, NJ). The elemental composition of the membrane surface was analyzed using X-ray photoelectron spectroscopy (XPS) with a PHI5000 VersaProbe III scanning XPS probe (Physical Electronics Inc., Chanhassen, MN, USA). Each XPS spectrum was collected over a sample area of 100 μm in diameter with 6 scans. XPS spectra were calibrated by setting adventitious C 1s binding energy at 284.8 eV. Atomic concentrations were calculated from the obtained XPS spectra using CasaXPS package and manufacturer-provided sensitivity factors. Deconvolution curves were fit by CasaXPS with consideration of peak position and full width at half-maximum. To determine the thickness of the PDA/GO and PDA/HGO layer, the membranes were immersed in DMF to dissolve the PES support, and the layer was kept on a mica substrate (Ted Pella, Inc., Redding, CA) followed by air drying. The thickness was obtained using the height profile measured by Atomic Force Microscope (AFM) (Bruker Dimension Icon with ScanAsyst, Bruker, Germany) in the tapping mode. Three AFM scans were taken for each sample, and three to four thickness measurements were performed in each AFM image. The final thickness was the average of the 9~12 measurements.

Water permeation tests, including pure water permeation, MWCO measurement, dye removal, and salt rejection, were conducted using dead-end filtration cells (UHP-25, Sterlitech, WA) at a feed pressure of 2.0 bar. Water permeance (A_w, LMH/bar) was calculated using Eq. (1) [15]:

$$A_w = \frac{V_w}{A_m \cdot t \cdot \Delta p} \tag{1}$$

where V_w (L) is the filtrate volume, A_m is the active membrane area (3.14 cm^2), t (h) is the filtration time, and Δp (bar) is the transmembrane pressure.

Methanol permeation test and DR 80 removal in methanol were performed using a high-pressure stirred cell (HP4750, Sterlitech) at a feed pressure of 1.22 bar. The methanol permeance (A_s) was calculated using the following equation:

$$A_s = \frac{V_s}{A_m \cdot t \cdot \Delta p} \tag{2}$$

where V_s (L) is the volume of the permeated methanol within the filtration time of t (h).

The MWCO was determined using aqueous solutions containing 1 g/L PEG with various molecular weights (M_W), including 1, 2, 4, 10, 20, 35, 100 kDa [39]. The filtration of a PEG solution was run for at least 30 min before collecting permeate samples to ensure a steady-state operation. The PEG content in the feed and permeate solutions was measured using a total organic carbon (TOC) analyzer (TOC-L, Shimadzu, JP). The rejection (R, %) was calculated using Eq. (3):

$$R = \left(1 - \frac{C_p}{C_f}\right) \times 100\% \tag{3}$$

where C_p and C_f are the PEG concentration in the permeate and feed, respectively. The nominal pore size of the membrane often equals the Stokes radius (a, nm) of the PEG with the rejection of 90% and the corresponding M_W. Eq. (4) is often used to estimate a [40]:

$$a = 16.73 \cdot 10^{-3} M_W^{0.557} \quad (4)$$

Dye removal efficiency is evaluated using 0.2 g/L dye solution (such as CR, DR 80, and MB), and the dye content in the solutions was determined using a UV–Vis spectrophotometer (UV-2600, Shimadzu, JP). Membranes were also challenged with 2 g/L Na_2SO_4 solutions to determine the salt rejection, and the salt content was determined using a conductivity meter (Vernier, OR). Due to the low Na_2SO_4 rejection for the membranes studied here, the osmotic pressure difference across the membrane is negligible compared with the transmembrane pressure.

The long-term stability of the membranes was tested using a constant-flux crossflow system [39, 40]. The feed pressure was kept constant, while the permeate pressure was varied to maintain the targeted permeate flux (controlled by a mass flow controller). The feed has a flow rate of 1 L/min and a Reynolds number of ≈900.

3. Results and discussion

3.1. Characterization of membrane nanostructures

Fig. 2a,b compares the SEM images of the GO and HGO nanosheets, validating that the etching decreases the size. More importantly, the etching creates 10-100 nm nanopores (as shown in the white dots in Fig. 3a). The nanopores were discussed in detail in our prior studies [15, 20] and other literature [38, 41], and they are not shown here for brevity. Fig. 2c-h confirms the deposition of PDA/HGO on the PES porous support by SEM. The surface pores on the PES support (Fig. 2c) disappear, and the surface becomes smooth after the deposition of PDA/HGO (Fig. 2d,e). The deposited layer can also be observed in the cross-section SEM images for PDA/HGO2h-30 and PDA/HGO4h-55, but not for other membranes with thinner selective layers because the featured laminar structure was too thin to visualize.

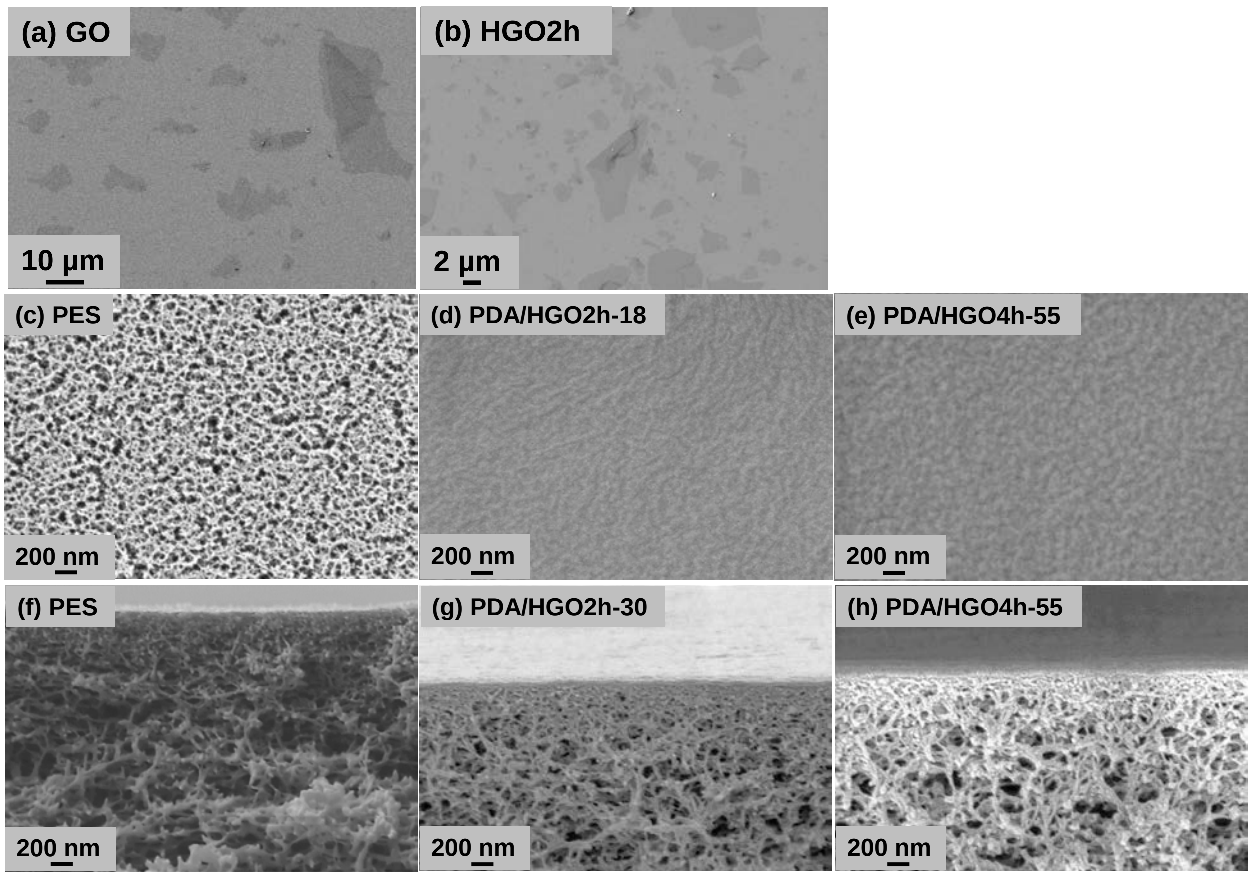

Fig. 2. SEM images of (a) GO and (b) HGO2h nanosheets. SEM images of the surface of (c) PES support, (d) PDA/HGO2h-18, and (e) PDA/HGO4h-55, and the cross-section of (f) PES support, (g) PDA/HGO2h-30, and (h) PDA/HGO4h-55.

The thickness of the selective layers was determined using AFM. The PES support was first dissolved using DMF, and the selective layer was transferred to a mica disc. The PDA/(H)GO appears to be stable in DMF, as validated by the large pieces of thin films (cf. Fig. S2) and consistent with the report of the excellent stability of PDA in DMF [42]. Fig. 3 presents the AFM results for an example membrane, PDA/GO-23. The step-change in the height profile can be ascribed to the thickness of the selective layer. Totally 10 to 12 thickness data for each sample were taken, and the average values are used. For PDA/HGO2h-30 and PDA/HGO4h-55, the thickness values from the AFM measurement are higher than those from the SEM cross-sectional images, presumably due to the difference in sample preparation and techniques.

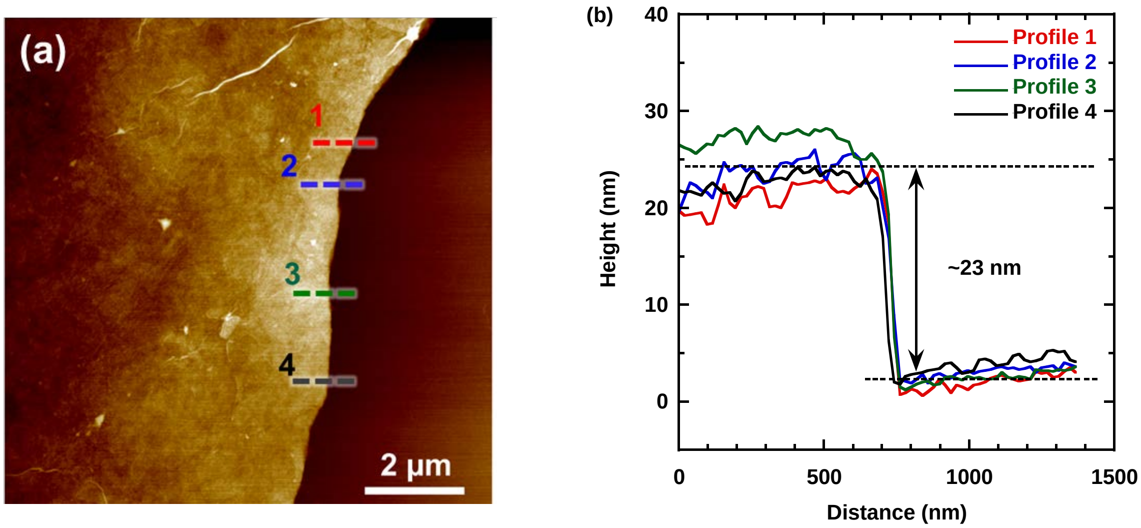

Fig. 3. (a) AFM image of the selective layer for PDA/GO-23. The blue, red, green, and pink marks label the four locations on the sample that were used for thickness measurement. (b) Height profile variance along the horizontal direction of the four measured locations.

XPS was used to determine the chemical composition of the materials used to form the membranes, including PDA, GO, and HGO, and the results are summarized in Table 1. PDA shows an N/C molar ratio of 0.095, which is lower than the theoretical value of 0.125 for pure dopamine but agrees well with the literature report for PDA [43]. GO and HGO do not have the N element, as expected. Additionally, GO exhibits an O/C ratio of 0.39, similar to HGO2h (0.37) and HGO (0.38), indicating that etching has a minimal effect on the chemical composition [15].

Table 1. The chemical composition of PDA, GO, HGO, and PDA/HGO membranes based on the XPS tests.

Samples	Atomic%			N/C molar ratio	O/C molar ratio	PDA content (mass%)
	C	O	N			
PDA	74.2	18.7	7.1	0.095	0.25	100
GO	71.7	28.3	0	0	0.39	0
HGO2h	72.9	27.1	0	0	0.37	0
HGO4h	72.6	27.4	0	0	0.38	0
PDA/GO-23	72.6	25.6	1.8	0.025	0.35	27
PDA/HGO2h-18	70.7	24.4	4.9	0.070	0.35	74
PDA/HGO2h-30	73.5	24.3	2.2	0.030	0.33	33
PDA/HGO4h-37	73.4	25.5	1.1	0.015	0.35	16
PDA/HGO4h-55	72.5	24.7	2.8	0.039	0.34	42

XPS was also used to determine the chemical composition of the selective layer surface. As shown in Table 1, the selective layer contains a significant amount of PDA (16-74 mass%), consistent with the literature [23]. However, there is no trend observed, and PDA/HGO2h-18 shows abnormally high estimated PDA content, presumably because the XPS only detects the top 2-5-nm layer, and there could be the randomness of different layers of HGO and PDA on the surface. Therefore, the PDA content in the whole selective layer may significantly deviate from these values.

All membranes show the values of the O/C molar ratio (0.33 – 0.35) slightly lower than that of GO or HGO (0.37 – 0.39), indicating that the PDA does not dramatically reduce the C-O or C=O groups in GO or HGO. The lower O/C molar ratio in the membranes can be caused by the lower value in PDA (0.25), instead of validating the claim that the PDA reduces the GO [23, 24]. Table S1 also shows the O/C ratio of the GO (or HGO) in the PDA/GO (or PDA/HGO) samples, which is very similar to that of the pure GO, further suggesting that the PDA does not reduce the GO or HGO. Additionally, high-resolution XPS spectra of C 1s for PDA, PDA/GO, and PDA/HGO were deconvoluted with the curve fittings shown in Figure S1, and the deconvolution results are summarized in Table S2.

The hydrophilicity of the membrane surface was characterized by the water contact angle. Fig. 4a shows that the deposition of the PDA/GO or PDA/HGO decreases the contact angle from 61^{o} for PES to 40^{o}, indicating the enhanced hydrophilicity, as the change is much more significant than the uncertainty (1 - 3^{o}). Additionally, the etching has a negligible effect on hydrophilicity. Both PDA/GO and PDA/HGO show the water contact angle similar to the GO/PES, suggesting that the PDA has a negligible impact on the surface hydrophilicity, as the PDA/PES also shows the water contact angle of 60^{o} - 70^{o} [43, 44]. The results also suggest that the PDA is much less hydrophilic than GO, consistent with the literature [24, 29, 34] but different from another study [31] presumably due to the different processing conditions.

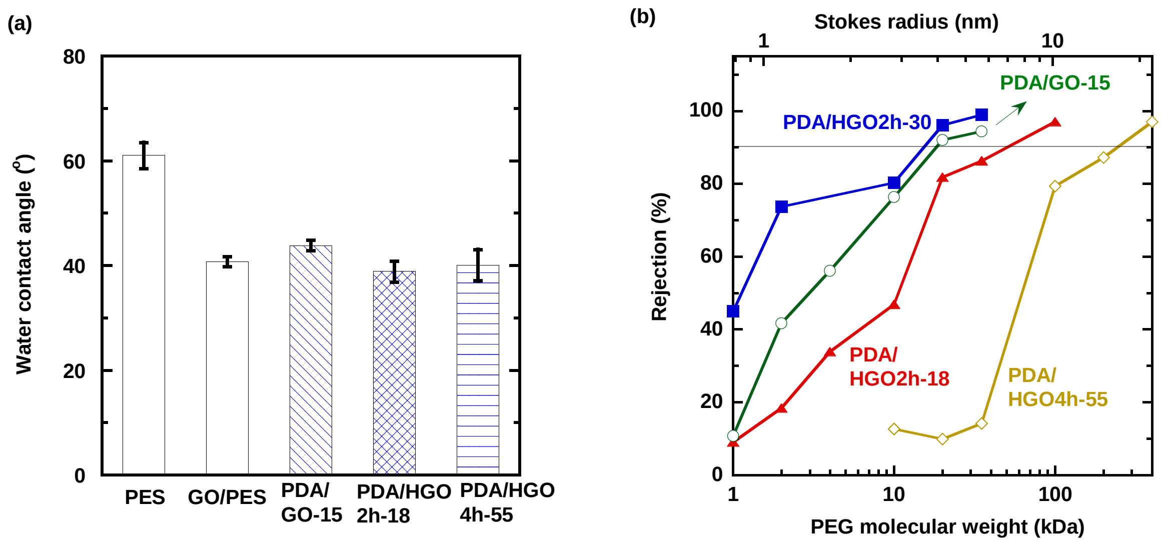

Fig. 4. (a) Water contact angle of PES support, GO/PES, PDA/GO-15, PDA/HGO2h-18, and PDA/HGO2h-55. (b) MWCO curves of PDA/GO and PDA/HGO membranes determined using 1 g/L PEG aqueous solutions with different molecular weights.

Fig. 4b displays the MWCO of the membranes determined using PEG with various molecular weights. The MWCO is defined as the molecular weight of the PEG with 90% rejection, and the nominal pore size of the membranes was estimated using the Stokes radius of the corresponding PEG molecule (cf. Tables S1 and 2) [40]. Despite their similar thickness of the selective layer, PDA/HGO2h-18 exhibits a larger MWCO than PDA/GO-15 because of the nanopores of the HGO nanosheets. Increasing the thickness of PDA/HGO2h decreases the MWCO due to the elimination of the voids or defects. For example, PDA/HGO2h-30 shows an MWCO of 19 kDa (with a nominal size of 4.0 nm), less than PDA/HGO2h-18 (58 kDa and 7.5 nm). Additionally, increasing the etching time increases the MWCO. For example, PDA/HGO4h-55 shows an MWCO of 257 kDa and a nominal size of 17 nm, much larger than PDA/HGO2h-30, which can be ascribed to the larger nanopores on the HGO sheets with increasing the etching time.

3.2. Separation performance of the PDA/HGO membranes

The effect of the composition and thickness of the selective layer of the membranes on the dye removal performance was systematically investigated. Fig. 5a and Table 2 present that the water permeance increases with decreasing the selective layer thickness and increasing the etching time (or density and size of the nanopores on the nanosheets [15]). For example, decreasing the thickness from 30 to 18 nm increases water permeance from 79 to 120 LMH/bar for PDA/HGO2h; increasing the etching time increases water permeance from 77 LMH/bar for PDA/GO-15 to 120 LMH/bar for PDA/HGO2h-18 and from 70 LMH/bar for PDA/HGO2h-30 to 460 LMH/bar for PDA/HGO4h-55 because of the decreased tortuosity, as shown by experimentation and modeling [15, 19, 20].

Fig. 5b displays the effect of the selective layer thickness on the CR rejection of the membranes. The thickness has a negligible effect on the CR rejection for PDA/GO. On the other hand, the CR rejection slightly increases from 98.5% to 99.5% as the thickness increases from 18 to 30 nm for PDA/HGO2h. PDA/HGO4h exhibits the rejection of < 90%, which is too low to be useful. The CR has a molecular size of 2.5 nm, and its rejection is higher than expected based on the MWCO values (4- 17 nm) of the membranes. Similar results have been observed in the literature, which is ascribed to the aggregation of the dye molecules [10, 45] and the overestimation of the MWCO because PEG molecules are linear and can deform to diffuse through channels smaller than their hydrodynamic diameter.

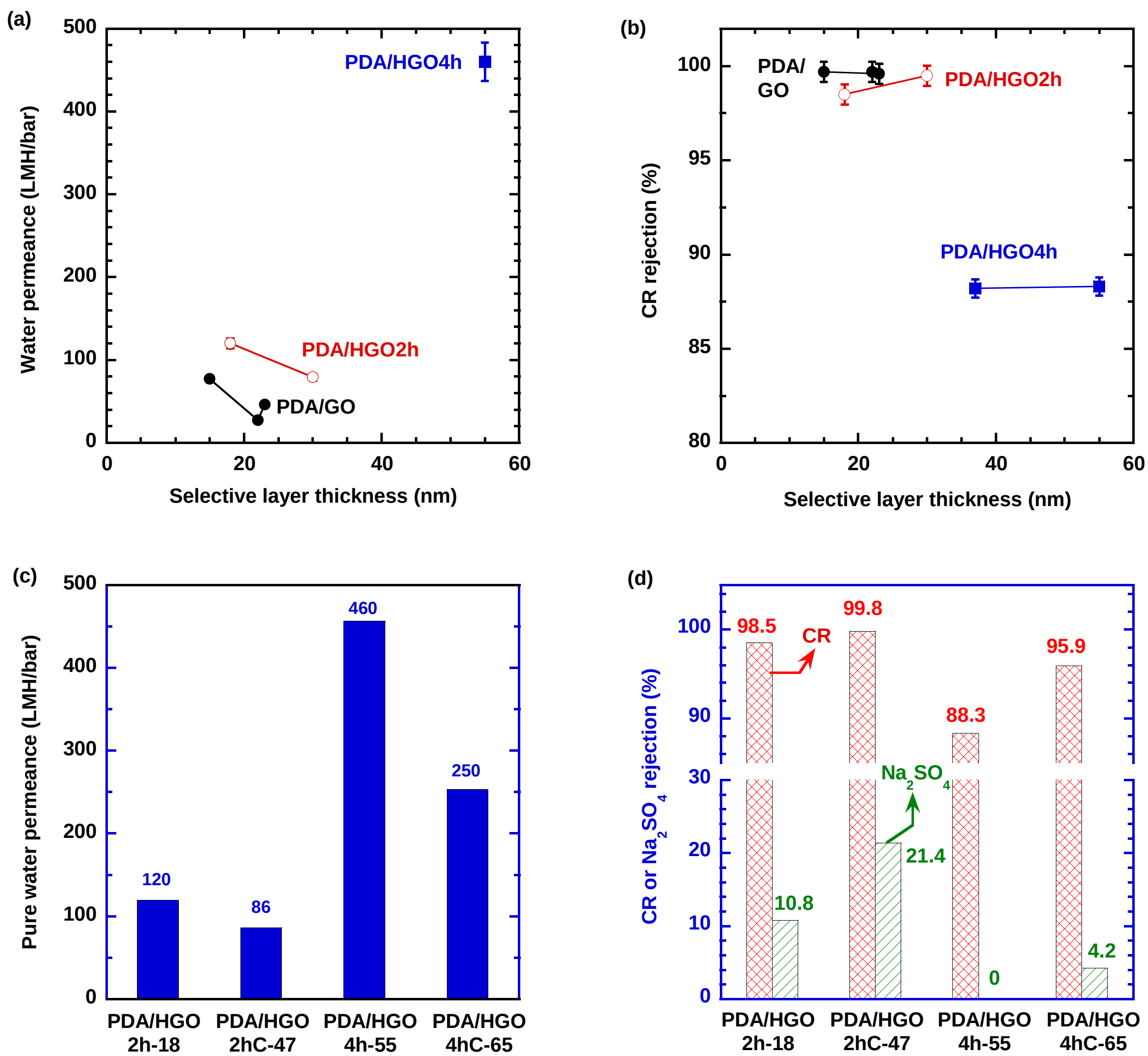

Fig. 5. Effect of the selective layer thickness on (a) water permeance and (b) CR rejection of PDA/GO, PDA/HGO2h, and PDA/HGO4h membranes when challenged with 0.2 g/L CR solutions at 2 bar. Effect of HGO centrifugation on (c) water permeance and (d) rejection of Na_2SO_4 and CR.

PDA/HGO2-18 exhibits water permeance of 120 LMH/bar (an order magnitude higher than that for commercial NF membranes [3] or tight UF membranes [10, 45] investigated for dye removal) and retention of 99.0% for DR80 (comparable to NF and tight UF membranes). Additionally, the PDA/HGO displays water permeance much higher than those prepared from PDA and GO (5.0 – 40 LMH/bar) [37, 46], demonstrating that the synergy of the GO etching and PDA intercalation improves the water permeance while retaining dye retention.

Table 2 records the water permeance and rejection to dyes or Na_2SO_4 for several representative membranes, as well as their nominal pore size. Na_2SO_4 is often used as a marker for other salts, as it has rejection much higher than NaCl and $MgCl_2$ and similar to $MgSO_4$ [2, 47, 48]. Increasing the HGO etching time from 2 to 4 h dramatically increases the water permeance to 460 LMH/bar (PDA/HGO4h-55), but it decreases the dye rejection to < 95%. These results are consistent with the MWCO data in Fig. 4b. The membranes exhibit better rejection to CR and DR 80 than MB because MB (with a size of 1.4 nm) is smaller than CR (2.5 nm) and DR 80 (4.4 nm) [3].

Table 2. Separation performance of representative PDA/GO and PDA/HGO membranes, including the average separation factor (α) for three dyes.

Membranes	a (nm)	A_W (LMH/ bar)	Rejection (%)				α of dye/ Na_2SO_4
			CR	DR 80	MB	Na_2SO_4	
PDA/GO-15	4.0	77±12	99.7±0.5	98.7±0.5	95.8±0.5	9.1±0.1	186
PDA/HGO2h-18	7.5	120±19	98.5±0.5	99.0±0.5	95.6±0.5	10.8±0.1	74
PDA/HGO2h-30	4.0	79±13	99.5±0.5	98.7±0.5	96.9±0.5	17.8±0.1	114
PDA/HGO4h-55	17	460±21	88.3±0.5	94.4±0.5	65.1±0.3	~0	13

The size of GO nanosheets plays an important role in determining the GO stacking structure and thus affects the separation performance [20, 21, 49]. To elucidate this effect, the aqueous dispersions of HGO were centrifuged to remove small debris before the fabrication of the membranes. Fig. 5c shows that the centrifugation of the HGO decreases water permeance and increases the rejection of dyes and Na_2SO_4. For example, PDA/HGO4hC-65 exhibits the CR rejection of 95.1%, higher than PDA/HGO4h-55 (88.3%). This agrees well with the previous findings that removing small pieces of GO nanosheets enhances the rejection by forming a well-packed laminar structure and decreases water permeance due to the increased tortuosity [15, 20].

The desalination performance can be characterized by separation factor (α), which is defined as the ratio of the salt permeation rate to the dye permeation rate and calculated using $\alpha = (1 - R_{salt})/(1 - R_{dye})$ [3]. Higher α values indicate better salt removal efficiency. Table 2 shows the compromise of the etching in improving water and salt permeance and decreasing dye rejection. PDA/HGO2h-18 exhibits higher water permeance but lower α than PDA/HGO-15, while increasing the PDA/HGO2h thickness decreases water permeance but increases α.

3.3. Continuous operation of the PDA/HGO membranes

To evaluate the feasibility of the HGO membranes for long-term operation, PDA/HGO2h-18 was challenged by three cycles of dye filtration tests using 200 ppm DR 80 and a constant-flux crossflow system. Each dye filtration test lasted for 3 h, followed by the membrane cleaning using NaOH solution (pH=11) for 0.75 h. The rejection to DR 80 was measured at the end of each filtration test. As shown in Fig. 6a, the rejection to DR 80 was greater than 99.4% in all three cycles, confirming the effectiveness of cleaning and the potential of the membranes for practical applications. The water permeance decreases slightly due to the fouling by the dye [31, 50], which can be partially mitigated by the NaOH cleaning. The stability of the membranes at high pH values is also consistent with a field study, which showed that the PDA-coated membranes were cleaned using acid or basic solutions without damage to the PDA layer [51].

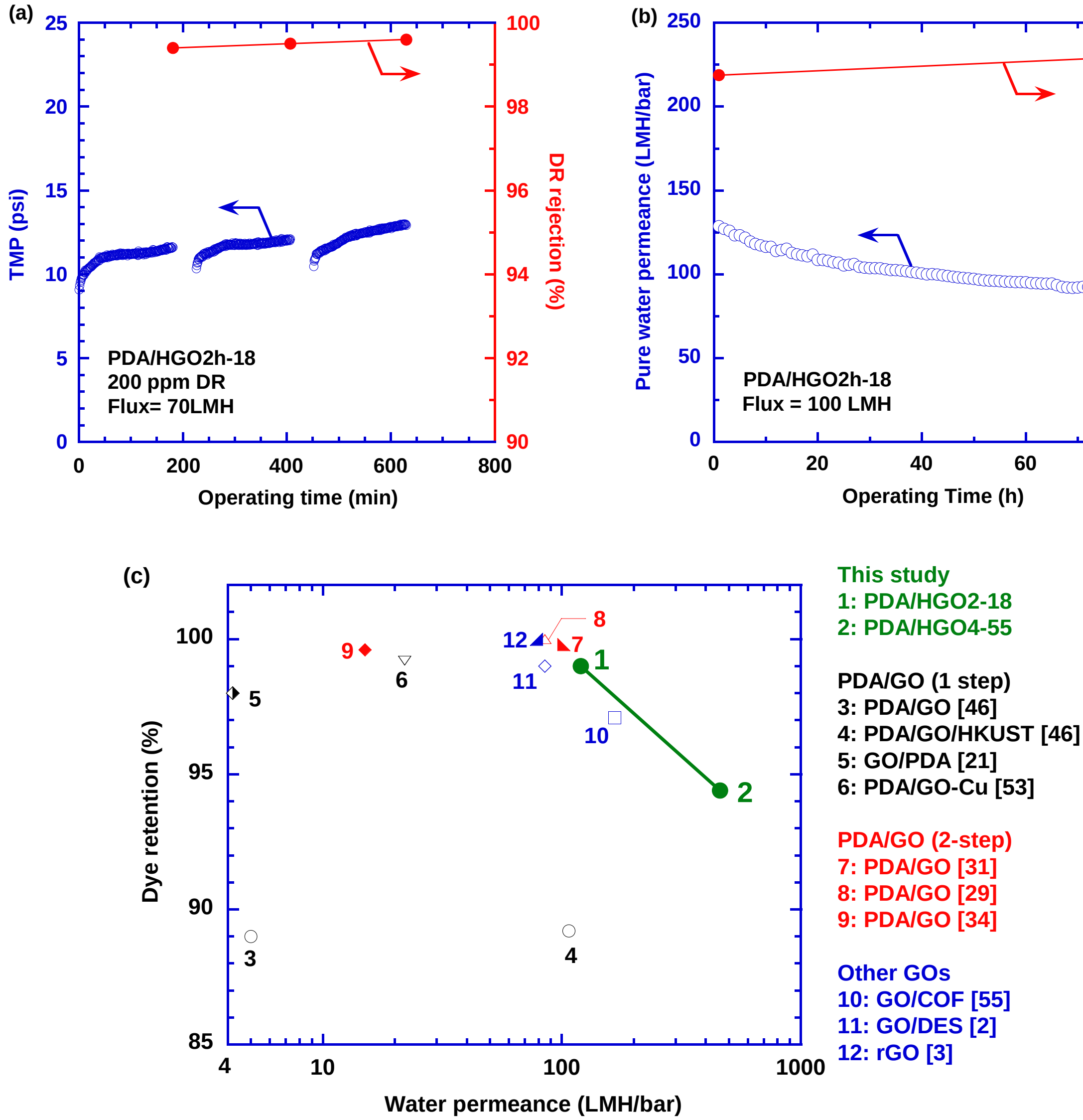

Fig. 6. (a) Multiple-cycle dye removal and membrane cleaning experiment conducted in a constant-flux crossflow system. (b) Long-term stability test for PDA/HGO2h-34 in the constant-flux system. (c) Comparison of the PDA/HGO membranes with GO-based membranes reported in the literature (cf. Table 2).

The stability of GO-based membranes in water is often a concern, especially when the membrane is operated in a crossflow system, and the shearing force can delaminate the HGO layer. Therefore, PDA/HGO2h-18 was challenged with a 3-day continuous filtration test with a Reynolds number of ≈900 to validate the stability of the membrane. As shown in Fig. 6b, the water permeance slightly decreases and then reaches a steady state. After the test, the membrane retains a high CR rejection of 99.3%, demonstrating the stability of the PDA/HGO membranes, which can be ascribed to the presence of PDA that reinforces the interaction between the HGO nanosheets [52]. Notably, the dye rejection values of ~99% indicate that some dye molecules can permeate through the membranes, and the permeated water may need further treatment using comprehensive process designs. However, this would be beyond the scope of this study.

Fig. 6c benchmarks the performance of our membranes with state-of-the-art PDA/GO membranes and other GO-based membranes reported in the literature (cf. Table 3). Our PDA/HGO membranes exhibit higher water permeance than those reported PDA/GO membranes. Moreover, the performance of our membranes is also among the best reported for GO-based membranes at comparable feed concentration, demonstrating the advantages of our NF membranes prepared by GO etching and PDA intercalation.

Table 3. Summary of dye removal performance of representative PDA/GO membranes and other GO-based membranes. Methylene Blue: MeB (320 Da); Rhodamine B: RB (479 Da); Direct Blue 14: DB 14 (961 Da).

Membrane components			Thickness (nm)	Preparation method	Dyes	A_W (LMH/Bar)	Dye *R* (%)	Na_2SO_4 *R* (%)	Ref.
GO	PDA	Others							
HGO2h	Yes	None	18	One-step codeposition	DR 80	120	99.0	10.8	This work
HGO4h	Yes	None	55	One-step codeposition	DR 80	460	94.4	~0	This work
GO	Yes	None	N/A	One-step codeposition	CR	5.0	~89	N/A	[46]
GO	Yes	HKUST-1	N/A	One-step codeposition	CR	107	89.2	N/A	[46]
GO	Yes	None	150	One-step codeposition	N/A	4.2	98	N/A	[21]
GO	Yes	None	~480	One-step codeposition	CR	60	97	N/A	[24]
GO	Yes	None	45	One-step codeposition	DR 80/CR	36.7	99.8	N/A	[37]
GO	Yes	$CuSO_4/H_2O_2$	N/A	One-step codeposition	CR	22	97.8	17	[53]
GO	Yes	Cu NPs	N/A	One-step codeposition	CR	22	99.2	8	[53]
GO	Yes	None	530	Two-steps	DB 14	100	99.8	N/A	[31]
GO	Yes	None	~75	Two-steps	CR	85	100	N/A	[29]
GO	Yes	None	126	Two-steps	MB	15	99.6	28	[34]
GO	No	COF-1	100-250	One-step	CR	31.1	99.6	5	[54]
GO	No	COF-TpPa	N/A	One-step	MeB	166.8	97.1	N/A	[55]
GO	No	CNT	N/A	One-step	CR	26.3	98.7	6.3	[56]
GO	No	DES	N/A	One-step	DR 80	85	99	20	[2]
rGO	No	None	~50	One-step	DR 80	80	99.99	~0	[3]

The potential of the PDA/HGO membranes for organic solvent filtration (OSN) was also evaluated [18, 57]. Pure methanol permeation and DR 80 removal in methanol were tested for PDA/HGO2h-18 using dead-end cells. As shown in Fig. 7a, the pure methanol permeance remains stable at 55 ± 4 LMH/bar for 1-h operation, which is lower than water permeance because of the larger molecular size of methanol than water. When challenged with DR 80 solutions, PDA/HGO2h-18 exhibits stable methanol permeance of ≈ 48 LMH/bar and DR 80 rejection of 97.7%~99.3% during the 3-h test. Interestingly, the dye rejection in methanol is similar to that in aqueous solutions, indicating that the nanochannels of the PDA/HGO layer remain similar in methanol and aqueous solutions. The stability of the PDA/HGO in methanol is also consistent with the literature, where PDA was synthesized from dopamine in methanol [58, 59].

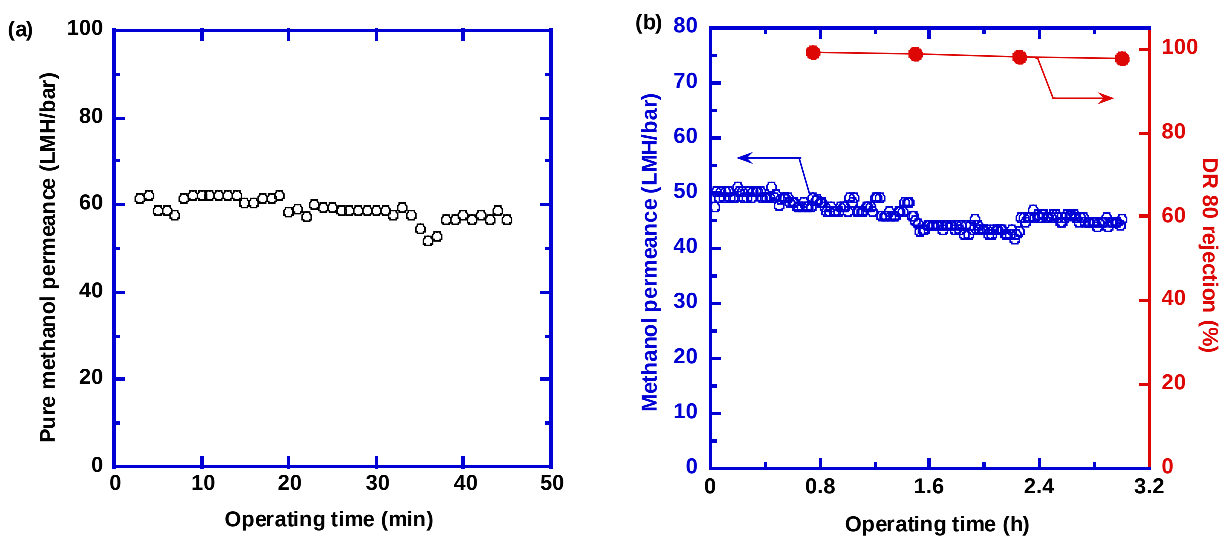

Fig. 7. (a) Pure methanol permeance of PDA/HGO2h-18 in the 45-min filtration at 1.22 bar. (b) DR 80 removal performance of PDA/HGO2h-18 in methanol at 1.22 bar during a multiple-cycle test conducted in a dead-end filtration system.

4. Conclusions

Chemical etching and PDA intercalation of GO nanosheets synergistically create nanochannels, leading to high water and salt permeance, high dye retention, and excellent stability. Etching introduces nanopores on the nanosheets (decreasing the tortuosity), and PDA intercalation increases interlayer spacings (and thus water permeance) and cross-links nanosheets (achieving stability). PDA also acts as an adhesive between the GO and porous support. The fabrication parameters (such as etching time, nanosheet size, and selective layer thickness) were facilely tuned to achieve a balance of water and salt permeance and dye retention. For example, centrifugation of HGO increases the nanosheet size and thus dye rejection while decreasing water permeance. PDA/HGO2h-18 display pure water permeance of 120 LMH/bar and CR rejection of 98.5%, much better than state-of-the-art commercial NF membranes and GO membranes reported in the literature. More importantly, the membrane exhibits stable performance after 72-h continuous filtration in a crossflow system, and the fouling can be partially mitigated by cleaning using NaOH solutions, demonstrating their potential for practical applications. This work unveils a versatile approach to tune the hierarchical nanochannels of membranes formed from other exciting 2D materials. Future work needs to focus on the manufacturing of the membranes on a large scale and demonstration of the performance for longer terms (such as 3 – 12 months) with simulated or real wastewater containing various salts and dyes.

Declaration of competing interest

The authors declare no conflict of interest.

Acknowledgment

We gratefully acknowledge the financial support from the U.S. Department of Energy (DOE) National Energy Technology Laboratory (DE-FE0031710) and the U.S. DOE Energy Efficiency & Renewable Energy (DE-EE0009500).

Appendix A. Supplementary Data

Supplementary data to this article can be found online.

References

[1] P. Jin, J. Zhu, S. Yuan, G. Zhang, A. Volodine, M. Tian, J. Wang, P. Luis, B. Van der Bruggen. Erythritol-based polyester loose nanofiltration membrane with fast water transport for efficient dye/salt separation. Chem. Eng. J. 406 (2021) 126796.

[2] N. Mehrabi, H. Lin, N. Aich. Deep eutectic solvent functionalized graphene oxide nanofiltration membranes with superior water permeance and dye desalination performance. Chem. Eng. J. 412 (2021) 128577.

[3] L. Huang, S. Huang, S. R. Venna, H. Lin. Rightsizing nanochannels in reduced graphene oxide membranes by solvating for dye desalination. Environ. Sci. Technol. 52 (2018) 12649-12655.

[4] R. Guo, T. Jiao, R. Li, Y. Chen, W. Guo, L. Zhang, J. Zhou, Q. Zhang, Q. Peng. Sandwiched Fe_3O_4/carboxylate graphene oxide nanostructures constructed by layer-by-layer assembly for highly efficient and magnetically recyclable dye removal. ACS Sustain. Chem. Eng. 6 (2018) 1279-1288.

[5] H. Guo, T. Jiao, Q. Zhang, W. Guo, Q. Peng, X. Yan. Preparation of graphene oxide-based hydrogels as efficient dye adsorbents for wastewater treatment. Nanoscale Res. Lett. 10 (2015).

[6] E. F. D. Januario, T. B. Vidovix, N. D. L. Beluci, R. M. Paixao, L. da Silva, N. C. Homem, R. Bergamasco, A. M. S. Vieira. Advanced graphene oxide-based membranes as a potential alternative for dyes removal: A review. Sci. Total Environ. 789 (2021) 147957.
[7] H. Park, J. Kamcev, L. M. Robeson, M. Elimelech, B. D. Freeman. Maximizing the right stuff: The trade-off between membrane permeability and selectivity. Science. 356 (2017) eaab0530.
[8] W. Ye, R. Liu, F. Lin, K. Ye, J. Lin, S. Zhao, B. Van der Bruggen. Elevated nanofiltration performance via mussel-inspired co-deposition for sustainable resource extraction from landfill leachate concentrate. Chem. Eng. J. 388 (2020) 124200.
[9] C. Liu, C. Wang, Y. Guo, J. Zhang, Y. Cao, H. Liu, Z. Hu, C. Zhang. High-performance polyamide membrane with tailored water channel prepared via bionic neural networks for textile wastewater treatment. J. Mater. Chem. A. 7 (2019) 6695-6707.
[10] M. Jiang, K. Ye, J. Deng, J. Lin, W. Ye, S. Zhao, B. Van der Bruggen. Conventional ultrafiltration as effective strategy for dye/salt fractionation in textile wastewater treatment. Environ. Sci. Technol. 52 (2018) 10698-10708.
[11] N. Yousefi, X. Lu, M. Elimelech, N. Tufenkji. Environmental performance of graphene-based 3D macrostructures. Nat. Nanotechnol. 14 (2019) 107-119.
[12] M. Hu, B. Mi. Enabling graphene oxide nanosheets as water separation membranes. Environ. Sci. Technol. 47 (2013) 3715-3723.
[13] T. Yang, H. Lin, K. P. Loh, B. Jia. Fundamental transport mechanisms and advancements of graphene oxide membranes for molecular separation. Chem. Mater. 31 (2019) 1829-1846.
[14] A. Morelos-Gomez, R. Cruz-Silva, H. Muramatsu, J. Ortiz-Medina, T. Araki, T. Fukuyo, S. Tejima, K. Takeuchi, T. Hayashi, M. Terrones. Effective NaCl and dye rejection of hybrid graphene oxide/graphene layered membranes. Nat. Nanotechnol. 12 (2017) 1083.
[15] X. Chen, Z. Feng, J. Gohil, C. M. Stafford, N. Dai, L. Huang, H. Lin. Reduced holey graphene oxide membranes for desalination with improved water permeance. ACS Appl. Mater. Interfaces. 12 (2020) 1387-1394.
[16] J. Zhu, J. Hou, A. Uliana, Y. Zhang, M. Tian, B. Van der Bruggen. The rapid emergence of two-dimensional nanomaterials for high-performance separation membranes. J. Mater. Chem. A. 6 (2018) 3773-3792.
[17] E. Igbinigun, Y. Fennell, R. Malaisamy, K. L. Jones, V. Morris. Graphene oxide functionalized polyethersulfone membrane to reduce organic fouling. J. Membr. Sci. 514 (2016) 518-526.
[18] L. Huang, Y. Li, Q. Zhou, W. Yuan, G. Shi. Graphene oxide membranes with tunable semipermeability in organic solvents. Adv. Mater. 27 (2015) 3797-3802.
[19] C. Buelke, A. Alshami, J. Casler, Y. Lin, M. Hickner, I. H. Aljundi. Evaluating graphene oxide and holey graphene oxide membrane performance for water purification. J. Membr. Sci. 588 (2019) 117195.

[20] L. Huang, W. Jia, H. Lin. Etching and acidifying graphene oxide membranes to increase gas permeance while retaining molecular sieving ability. AIChE J. 66 (2020) e17022.
[21] M. Zhang, Y. Mao, G. Liu, G. Liu, Y. Fan, W. Jin. Molecular bridges stabilize graphene oxide membranes in water. Angew. Chem. Int. Ed. 59 (2020) 1689-1695.
[22] L. Huang, J. Chen, T. Gao, M. Zhang, Y. Li, L. Dai, L. Qu, G. Shi. Reduced graphene oxide membranes for ultrafast organic solvent nanofiltration. Adv. Mater. 28 (2016) 8669-8674.
[23] L. Xu, W. Yang, K. G. Neoh, E. Kang, G. Fu. Dopamine-Induced Reduction and Functionalization of Graphene Oxide Nanosheets. Macromolecules. 43 (2010) 8336-8339.
[24] J. Ma, Y. He, G. Zeng, F. Li, Y. Li, J. Xiao, S. Yang. Bio-inspired method to fabricate polydopamine/reduced graphene oxide composite membranes for dyes and heavy metal ion removal. Polym. Adv. Technol. 29 (2018) 941-950.
[25] V. Agarwal, P. B. Zetterlund. Strategies for reduction of graphene oxide - A comprehensive review. Chem. Eng. J. 405 (2021) 127018.
[26] L. Chen, G. Shi, J. Shen, B. Peng, B. Zhang, Y. Wang, F. Bian, J. Wang, D. Li, Z. Qian, G. Xu, G. Liu, J. Zeng, L. Zhang, Y. Yang, G. Zhou, M. Wu, W. Jin, J. Li, H. Fang. Ion sieving in graphene oxide membranes via cationic control of interlayer spacing. Nature. 550 (2017) 415-418.
[27] H. Lee, S. M. Dellatore, W. M. Miller, P. B. Messersmith. Mussel-inspired surface chemistry for multifunctional coatings. Science. 318 (2007) 426-430.
[28] N. Shahkaramipour, A. Jafari, T. Tran, C. M. Stafford, C. Cheng, H. Lin. Maximizing the grafting of zwitterions onto the surface of ultrafiltration membranes to improve antifouling properties. J. Membr. Sci. 601 (2020) 117909.
[29] C. Wang, Z. Li, J. Chen, Y. Yin, H. Wu. Structurally stable graphene oxide-based nanofiltration membranes with bioadhesive polydopamine coating. Appl. Surf. Sci. 427 (2018) 1092-1098.
[30] Y. Li, S. Shi, H. Gao, Z. Zhao, C. Su, H. Wen. Improvement of the antifouling performance and stability of an anion exchange membrane by surface modification with graphene oxide (GO) and polydopamine (PDA). J. Membr. Sci. 566 (2018) 44-53.
[31] Y. Zhan, X. Wan, S. He, Q. Yang, Y. He. Design of durable and efficient poly(arylene ether nitrile)/bioinspired polydopamine coated graphene oxide nanofibrous composite membrane for anionic dyes separation. Chem. Eng. J. 333 (2018) 132-145.
[32] W. Zhong, Y. Zhang, L. Zhao, W. Li. Highly stable and antifouling graphene oxide membranes prepared by bio-inspired modification for water purification. Chin. Chem. Lett. 31 (2020) 2651-2656.
[33] N. K. Khanzada, S. Rehman, S.-Y. Leu, A. K. An. Evaluation of anti-bacterial adhesion performance of polydopamine cross-linked graphene oxide RO membrane via in situ optical coherence tomography. Desalination. 479 (2020) 114339.

[34] Y. Xu, M. Wu, S. Yu, Y. Zhao, C. Gao, J. Shen. Ultrathin and stable graphene oxide film via intercalation polymerization of polydopamine for preparation of digital inkjet printing dye. J. Membr. Sci. 586 (2019) 15-22.

[35] R. Xing, W. Wang, T. Jiao, K. Ma, Q. Zhang, W. Hong, H. Qiu, J. Zhou, L. Zhang, Q. Peng. Bioinspired polydopamine sheathed nanofibers containing carboxylate graphene oxide nanosheet for high-efficient dyes scavenger. ACS Sustain. Chem. Eng. 5 (2017) 4948-4956.

[36] F. Li, Z. Yu, H. Shi, Q. Yang, Q. Chen, Y. Pan, G. Zeng, L. Yan. A Mussel-inspired method to fabricate reduced graphene oxide/g-C_3N_4 composites membranes for catalytic decomposition and oil-in-water emulsion separation. Chem. Eng. J. 322 (2017) 33-45.

[37] L. Liu, X. Xie, R. S. Zambare, A. P. J. Selvaraj, B. N. Sowrirajalu, X. Song, C. Y. Tang, C. Gao. Functionalized graphene oxide modified polyethersulfone membranes for low-pressure anionic dye/salt fractionation. Polymers. 10 (2018) 795.

[38] Y. Xu, C.-Y. Chen, Z. Zhao, Z. Lin, C. Lee, X. Xu, C. Wang, Y. Huang, M. I. Shakir, X. Duan. Solution processable holey graphene oxide and its derived macrostructures for high-performance supercapacitors. Nano Lett. 15 (2015) 4605-4610.

[39] X. Chen, E. Deng, D. Park, B. A. Pfeifer, N. Dai, H. Lin. Grafting activated graphene oxide nanosheets onto ultrafiltration membranes using polydopamine to enhance antifouling properties. ACS Appl. Mater. Interfaces. 12 (2020) 48179-48187.

[40] T. Tran, Y.-C. Tu, S. Hall-Laureano, C. Lin, M. Kawy, H. Lin. “Nonstick” membranes prepared by facile surface fluorination for water purification. Ind. Eng. Chem. Res. 59 (2020) 5307-5314.

[41] J. Yang, X. Shan, Z. Guo, L. Duan, X. Zhang, W. Lu. A facile synthetic strategy of free-standing holey graphene paper as sulfur host for high-performance flexible lithium sulfur batteries. J. Electroanal. Chem. 876 (2020) 114728.

[42] D. Zhao, J. Kim, G. Ignacz, P. Pogany, Y. Lee, G. Szekely. Bio-inspired robust membranes nanoengineered from interpenetrating polymer networks of polybenzimidazole/polydopamine. ACS Nano. 13 (2019) 125-133.

[43] N. Shahkaramipour, S. N. Ramanan, D. Fister, E. Park, S. R. Venna, H. Sun, C. Cheng, H. Lin. Facile grafting of zwitterions onto the membrane surface to enhance antifouling properties for wastewater reuse. Ind. Eng. Chem. Res. 56 (2017) 9202-9212.

[44] B. D. McCloskey, H. Park, H. Ju, B. W. Rowe, D. J. Miller, B. J. Chun, K. Kin, B. D. Freeman. Influence of polydopamine deposition conditions on pure water flux and foulant adhesion resistance of reverse osmosis, ultrafiltration, and microfiltration membranes. Polymer. 51 (2010) 3472-3485.

[45] J. Lin, W. Ye, M. C. Baltaru, Y. Tang, N. J. Bernstein, P. Gao, S. Balta, M. Vlad, A. Volodin, A. Sotto, P. Luis, A. L. Zydney, B. Van der Bruggen. Tight ultrafiltration membranes for enhanced separation of dyes and Na_2SO_4 during textile wastewater treatment. J. Membr. Sci. 514 (2016) 217-228.

[46] Y. Liu, M. Zhu, M. Chen, L. Ma, B. Yang, L. Li, W. Tu. A polydopamine-modified reduced graphene oxide (RGO)/MOFs nanocomposite with fast rejection capacity for organic dye. Chem. Eng. J. 359 (2019) 47-57.

[47] A. Metecan, A. Cihanoglu, S. A. Altinkaya. A positively charged loose nanofiltration membrane fabricated through complexing of alginate and polyethyleneimine with metal ions on the polyamideimide support for dye desalination. Chem. Eng. J. 416 (2021) 128946.

[48] X. Wei, X. Kong, C. Sun, J. Chen. Characterization and application of a thin-film composite nanofiltration hollow fiber membrane for dye desalination and concentration. Chem. Eng. J. 223 (2013) 172-182.

[49] F. Perreault, A. F. de Faria, S. Nejati, M. Elimelech. Antimicrobial properties of graphene oxide nanosheets: Why size matters. ACS Nano. 9 (2015) 7226-7236.

[50] L. Zhu, M. Wu, B. Van der Bruggen, L. Lei, L. Zhu. Effect of TiO_2 content on the properties of polysulfone nanofiltration membranes modified with a layer of TiO_2–graphene oxide. Sep. Purif. Techn. 242 (2020) 116770.

[51] D. J. Miller, X. Huang, H. Li, S. Kasemset, A. Lee, D. Agnihotri, T. Hayes, D. R. Paul, B. D. Freeman. Fouling-resistant membranes for the treatment of flowback water from hydraulic shale fracturing: A pilot study. J. Membr. Sci. 437 (2013) 265-275.

[52] A. Deshmukh, C. Boo, V. Karanikola, S. H. Lin, A. P. Straub, T. Z. Tong, D. M. Warsinger, M. Elimelech. Membrane distillation at the water-energy nexus: limits, opportunities, and challenges. Energy Environ. Sci. 11 (2018) 1177-1196.

[53] J. Zhu, J. Wang, A. A. Uliana, M. Tian, Y. Zhang, Y. Zhang, A. Volodin, K. Simoens, S. Yuan, J. Li, J. Lin, K. Bernaerts, B. Van der Bruggen. Mussel-inspired architecture of high-flux loose nanofiltration membrane functionalized with antibacterial reduced graphene oxide–copper nanocomposites. ACS Appl. Mater. Interfaces. 9 (2017) 28990-29001.

[54] X. Zhang, H. Li, J. Wang, D. Peng, J. Liu, Y. Zhang. In-situ grown covalent organic framework nanosheets on graphene for membrane-based dye/salt separation. J. Membr. Sci. 581 (2019) 321-330.

[55] G. Kong, J. Pang, Y. Tang, L. Fan, H. Sun, R. Wang, S. Feng, Y. Feng, W. Fan, W. Kang, H. Guo, Z. Kang, D. Sun. Efficient dye nanofiltration of a graphene oxide membrane via combination with a covalent organic framework by hot pressing. J. Mater. Chem. A. 7 (2019) 24301-24310.

[56] L. Huang, Z. Li, Y. Luo, N. Zhang, W. Qi, E. Jiang, J. Bao, X. Zhang, W. Zheng, B. An, G. He. Low-pressure loose GO composite membrane intercalated by CNT for effective dye/salt separation. Sep. Purif. Techn. 256 (2021) 117839.

[57] A. Tandel, W. Guo, K. Bye, L. Huang, M. Galizia, H. Lin. Designing organic solvent separation membranes: polymers, porous structures, 2D materials, and their combinations. Mater. Adv. 2 (2021) 4574-4603.

[58] I. You, H. Jeon, K. Lee, M. Do, Y. Seo, H. Lee, H. Lee. Polydopamine coating in organic solvent for material-independent immobilization of water-insoluble molecules and avoidance of substrate hydrolysis. J. Ind. Eng. Chem. 46 (2017) 379-385.

[59] X. Jiang, Y. Wang, M. Li. Selecting water-alcohol mixed solvent for synthesis of polydopamine nano-spheres using solubility parameter. Sci. Rep. 4 (2014) 6070.